



Finite Element Simulation for Thermo-Mechanical Transient Behavior of Mild Steel Plate Agglutinated by Gas Tungsten Arc Welding (GTAW) Technique

Michael Okon Bassey^{a*}, Umoh Offiong^a, Aniekan Essienubong Ikpe^b

^a Akwa Ibom State Polytechnic, Department of Mechatronics Engineering, PMB. 1200, Nigeria

^b Akwa Ibom State Polytechnic, Department of Mechanical Engineering, PMB. 1200, Nigeria

*Michael.bassey@akwaibompoly.edu.ng

ARTICLE INFORMATION

Article history:

Received 30 July 2023

Revised 12 August 2023

Accepted 15 August 2023

Available online 29 August 2023

Keywords:

Welding, Thermal cycle, Yield strength, Simulation, Mild steel, Experimental approach.

<https://doi.org/10.5281/zenodo.8306756>

ISSN-1115-5825/© 2023NIPES Pub. All rights reserved

ABSTRACT

Finite element approach was employed in this study to simulate the thermo-mechanical transient behavior of mild steel plate agglutinated by gas tungsten arc welding (GTAW) technique. This was achieved through computational modelling and experimental technique. It was observed that most of the heat transfer occurred around the fusion zone via conduction. However, not all of the 100% heat was transferred to the weld pool due to heat losses taking place during heat transfer. The strength of the weld deposit increased with lower heat inputs, although this also varied greatly as a result of the variable welding inputs employed in the welding sequence. Therefore, applying lower heat input can improve the tensile yielding effect of the material. It was observed that each finite element profile model had a region characterized by minimum and maximum welding temperature and yield strength which revealed that maximum temperature and maximum yield strength (tensile) value both occurred around the welded region or fusion zone, indicating that the fusion zone is stronger than the parent metal. Yield strength of the AISI 1018 mild steel plate before welding operation was obtained as 370MPa, which is quite lower than that obtained after welding. The study also revealed the correlation between FEM modelled and experimentally determined output parameters, as maximum FEM and experimental yield strength values of 478.724 and 470.713MPa were produced by welding temperature of 1391 and 1406°C. The findings revealed that FEM is an effective tool that can adequately model and simulate the thermo-mechanically related material thermal cycle and yield strength.

1. Introduction

Welding is considered as the most critical part of fabrication process that is employed in the manufacturing and construction industries. Numerous welding methods have been created over time to meet the ever-changing needs and to stay up with the development of new materials. The success of any welding operation depends on a variety of input parameters and how they interact with the

material's qualities and the weld quality that can be achieved. These parameters range from the input current, voltage and the gas flow rate [1]. A common method for combining metal components that are comparable and dissimilar is gas tungsten arc welding (GTAW), which is better suited for joining metals and their alloys [2]. The thermoplastic strain produced during the course of this operation in the body as a result of the sharp temperature differential and the strains caused by phase transitions during a thermal cycle are the main causes of residual stresses and strains in these sections. Reduced structural integrity is caused by residual stress surrounding welds [3].

Consequently, it is crucial for designers to anticipate post-welding structure circumstances including residual strains, distortions and deformation. Previously, experimental measuring techniques which were frequently expensive and time-consuming were deployed to compute the welding residual stresses. Therefore, employing mathematical techniques like the finite element method (FEM), researchers sought to estimate remaining stresses and deformation over the previous few decades [4, 5]. However, the behaviour of intricate structural components and processes can be studied and predicted using the effective numerical simulation technique such as finite element analysis (FEM). Wu et al. [6] in their experimental study reported a novel model to evaluate the phase changes during welding operation under fusion process and it synthesised the residual strain which was alluded to the deploying of GTAW process. They established that the inclusion of phase transitions has a large impact on residual stresses in medium- and high-carbon steel, it has a very minimal impact on low-carbon steel like AISI 1020. Chang and Teng [7] also in their investigative study on the thermo-mechanical behaviour and estimation of residual stresses in welded butt joints using thermal elastic-plastic analysis utilizing the finite element method (FEM). Additionally, they calculated surface residual stresses using the X-ray diffraction technique and contrasted them with the outcomes of the simulation. They modelled a three-pass GTAW using the element's birth and death properties.

Ikpe and Bassey [8] also deployed FEM in the simulation of AISI 1018 10mm flat steel plate under a tungsten inert gas operation. The deployment of the FEM proved useful in the thermal analysis and the residual stresses that originated from the heat affected zone (HAZ) and followed by the heat that originated from the weldment and the entire plate. The resulting effect showed clearly that the stress impact centred on the contours of the weldment. In the same vein, it was further observed that von-mises (at highest stress point) stress concentrated at the sharp edges which divided the vertical and horizontal planes of the work piece (steel flat plate).

Mohan and Shanmugam [9] conducted an experimental and Finite Element (FE) analysis on the mechanical behaviour of AISI 321 plate samples (base metal and weld metal) by performing a uniaxial tensile and Charpy impact test. The results of stress-strain values and impact energy predicted by the FE analysis agree with experimental results. Also, the fracture behaviour of the experimental and FE simulations was identical to ductile mode of fracture. In the FE analysis, the neck and fracture locations of the base metal and weld metal samples were very similar to the experiment.

Coz Díaz et al. [10] analysed TIG welding distortions between Austenitic and Duplex Stainless Steels using FEM. The FEM including the birth and death technique was observed as an efficient procedure to analyse the vertical displacement evolution at different plate locations in the welding process of stainless steels, as well as their angular deformation and longitudinal bending. Comparatively, there was a significant agreement between the FEM numerical and experimental results.

To determine the effect of TIG welding on the thermomechanical performance of AISI 304 butt joints, Bash [11] employed a 3D analysis with non-linear thermo-mechanical simulations for AISI 304 stainless steel using finite element analysis to determine the failure mode of butt joints under tensile stress test. The study revealed that welding current increased with increase in the heat input, resulting in decrease on the fusion zones. This led to a reduction in the cooling rate and an increase

in the grain size of the weld metal and the region affected by HAZ. An increase in welding current also resulted in an increase along the width of the HAZs and increase in the volume fraction as well as decrease in microhardness of the weld samples. The results indicated that the longitudinal residual stress distribution is uniform along the weld line with similar pattern with transversal residual stress. A 3D finite element (FE) analysis was carried out by Jiang et al. [12] using the double distribution of Goldak ellipsoidal heat source. The fields of residual stress and temperature in welds repair stainless steel plates had been considered in the study. The results indicated that the length of the repair had effects on transverse stress, longitudinal stress and yield strength of the welds and HAZs.

Numerical study was conducted by Chen et al. [13] on the effect of welding process on the stress-strain relation with tensile strength of high strength steel grade S690Q. The results revealed that increase in butt joint thickness resulted in a decrease in the joint strength under direct tensile test, and this was achieved when the passing heat was constantly maintained.

The out-of-plane distortion of a thin plate during the Tungsten Inert Gas (TIG) welding process was determined by Huang [14], using the Digital Image Correlation (DIC) and FEM for determining the geometric imperfections. The numerical results and experimental data correlated in both out-of-plane deformation modes and magnitudes of the plate at each category of welding. The maximum out-of-plane distortion was larger than 4 mm during welding which resulted in instability of arc length and heat input.

A three-dimensional finite element welding simulation was carried out by Musa et al. [15] on a one pass Manual Metal Arc Welding plain joint structure. The comparison of the residual stresses (transverse and longitudinal) determined by the finite element method and X-Ray diffraction experiment indicated a fair agreement with the experimental results.

A finite element (FE) thermo-mechanical model was employed by García-García et al. [16] to analyse welding thermal cycle in the TWIP-Ti steel. The magnitude of residual stresses estimated in the Stress Critical Zone (SCZ) was lower than the TWIP-Ti steel yield strength. The multilinear kinematic model with a strain rate of 0.01 s^{-1} was the average condition that accurately simulated residual stress and deformation distributions during the welding thermal cycle in the present TWIP-Ti steel. The weld joint preparation and the mechanical constraint provided a control to mitigate both residual stress and distortion.

In this present study, our focus is premised on the finite element simulation for thermo-mechanical transient behaviour of mild steel plate agglutinated by GTAW technique. The nonlinear non-coupled thermal and mechanical solution will be employed to simulate the welding process in two steps. The thermal solution and mechanical solution, respectively, which yield the thermal history and stresses distribution. The outcomes of the simulation software, those of the research experiments, and the outcomes provided by other researchers will be compared for validation.

2. Materials and Method

The specific objective of the study was to optimize the welding input variables for desired welding output responses. The final solution of the optimization process was to determine the optimum values of the input variables (current, voltage, gas flow rate and welding speed) that can produce optimum welding temperature and maximum yield strength. The randomized design matrix comprised of four input variables namely: current (Amp), voltage (V), gas flow rate (L/min) and welding speed, with two output responses namely: welding temperature and yield strength. To generate experimental data for the optimization, process the following steps were adopted:

- i. Statistical design of experiment (DOE) using the central composite design (CCD) method was carried out. The CCD is one of the most acceptable design for response surface methodology (RSM) [17, 18]. The design and optimization was done using statistical software and for this particular problem, Design Expert 7.01 was used.
- ii. Design Expert 7.01 software was used to generate design of experiment (DOE) for twenty (20) (having six (6) centre points, six (6) axial points and eight (8) factorial points) experimental runs (see Table 1) as input parameters for experimental TIG welding procedure and FEM prediction and optimization. However, the same DOE employed by Owunna and Ikpe [19] in a study on experimental and numerical optimization of TIG welding process parameters relative to mechanical properties (UTS, yield strength, strain and elongation) of AISI 1018 mild steel plate was also adopted in this study.

Table 1: Welding Parameters from design of experiment

Weld Runs	Current (amps)	Voltage (V)	Gas flow rate (litters/min)	Welding speed (mm/min)
1	180	21.00	19.00	3.75
2	183	18.00	19.00	3.75
3	185	18.50	19.00	3.75
4	190	19.00	19.00	3.75
5	195	21.50	19.00	3.75
6	200	20.00	19.00	3.75
7	205	20.50	19.00	3.75
8	210	21.00	19.00	3.75
9	213	18.00	19.00	3.75
10	215	18.50	19.00	3.75
11	218	19.00	19.00	3.75
12	221	21.50	19.00	3.75
13	225	20.00	19.00	3.75
14	225	20.50	19.00	3.75
15	240	21.00	19.00	3.75
16	228	18.00	19.00	3.75
17	230	18.50	19.00	3.75
18	230	19.00	19.00	3.75
19	235	21.50	19.00	3.75
20	225	20.00	19.00	3.75

Ten millimeter (10 mm) plate was obtained from Universal Steel Rolling Mill, Ogba-Ikeja, Lagos, Nigeria, and analysis for mechanical properties and chemical composition, which revealed that the material is AISI 1018 low carbon steel was determined in the same company using mass analyzer. The mechanical properties and composition of the AISI 1018 mild steel plate are presented in Table 2. The 10 mm steel plate was cut into 60 x 40 x 10 mm (length x width) pieces. Emery paper was used to smoothen each of the two specimen to eliminate all possible coatings, corrosion or rust that may have accumulated on the material. AISI 1018 is mild/low carbon steel with carbon composition ranging from 0.14-0.20%, 98.81-99.26% of iron, 0.60-0.90% of manganese, ≤0.040% of phosphorous, , ≤0.050% of Sulphur etc [20], and has excellent weldability. It can be welded instantly by several conventional welding methods, and produces a uniform harder case which is the reason why it is considered one of the best steel material for carburized parts [21], but welding of AISI 1018 steel is however not recommended when it is carbonitrided. It offers a good balance of toughness, strength and ductility, and can be welded with low carbon welding electrode without post-heating and pre-heating.

Table 2: Properties and composition of AISI 1018 mild steel plate

Mechanical properties	Chemical compositions
-----------------------	-----------------------

Hardness (Brinell)	126 N/mm ²	Carbon	0.14-0.20 %
Tensile strength (Yield)	370 MPa	Iron	98.81-99.26 %
Ultimate Tensile strength	440.507 MPa	Manganese	0.60-0.90 %
Elastic modulus	205 GPa	Phosphorous	≤ 0.040 %
Poisson's ratio	0.290	Sulphur	≤ 0.050 %
Mass density	7.87 g/cc	Silicon	0.10 %
Shear modulus	80mGPa	Molybdenum	0.15-0.25 %
Thermal expansion coefficient	1.5e-005 /Kelvin	Silicon	0.020%

The two steel plates were chamfered at 30 degrees, after which, fusion welding was used to join the two plates together to form an angle of 60 degrees with 2mm depth. Prior to welding, surface of the samples to be welded were chemically cleaned with acetone to eliminate surface contamination and welding was applied on the flat plates to fill the chamfered V-groove using the welding parameters in Table 1.

The welding torch passed over the plate at a height of 2.5mm from the workpiece at constant velocity of 1.72 mm/s⁻¹. Attached to the surface of the work piece were Type-K thermocouple which allowed the temperature gradient to be recorded at intervals as the arc transverse across the work specimen. After welding, surface of the 10 mm flat plates were prepared again through grinding, degreasing, abrading, conditioning and neutralizing. Some materials used in the process were vice, hack saw, angle grinding machine, wire brush, file, enchant chemical etc.

Grinding was done with the help of a grinding machine to remove spatters from the surface of the plate, degreasing was done by using GC-6 Isopropyl alcohol and gauze sponge to clean the surface of the beam in order to remove oil, grease and other contaminants from the surface of the metal plate. The surface was then wetted with mild acidic solution and then abraded again using a smooth emery paper to remove any other scales and oxides found on the surface of the plate. The application of mild acidic solution was to enhance the cleaning process. After abrading, the surface was again cleaned with gauze sponge and alcohol. A basic solution (M-pep neutralizer 5A) was then applied to neutralize the surface after which the surface was dried with gauze sponge. This procedure was repeated for 20 pieces of 10 mm flat steel plates which were now ready to be subjected to tensile test. Prior to subjecting the samples to welding, tensile test was carried out on the original AISI 1018 plate to determine the yield strength of the material. The idea was to compare the yield strength of the material before and after welding in order to determine the variations. Figure 1a represents unprepared samples with v-groove, Figure 1b represents polished samples and Figure 1c represents the welded samples.

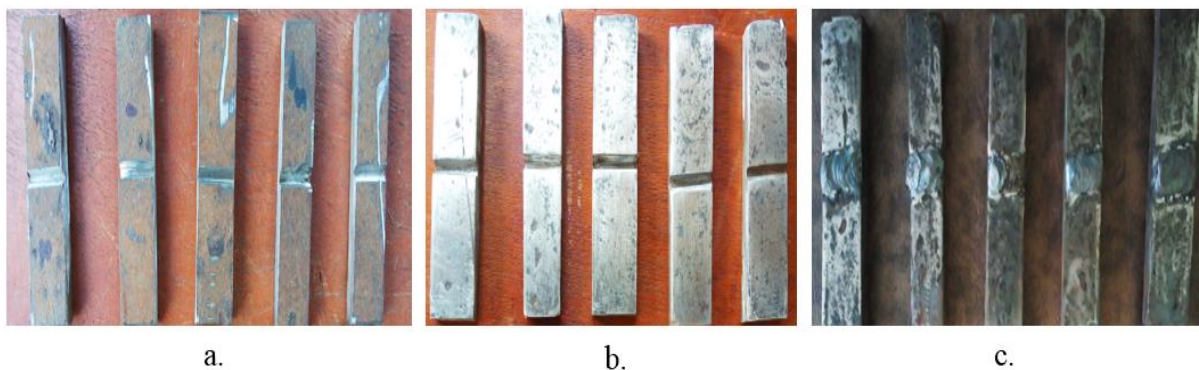


Figure 1. Low carbon steel plate samples used for the experimental procedure

Strain gauge rosette was attached on the weldment, with lead wires soldered on it while the other ends were connected to the input terminals (channels) of P3 Strain Indicator. A transparent glass shield was used to shield off the INSTRON machine to prevent the specimen from hitting anyone should it accidentally go off the machine during the test. The INSTRON tensile machine was

switched on, the gauge meter was reset to zero to ensure the equipment does not display wrong data and a force ranging from 12,000-20,000 N was applied gradually on the flat plate until it yielded and failed. The yield strength which each loaded sample yielded was recorded. The yield strength is the force required to cause a material to plastically deform or yield. The twenty flat plate specimens were mounted on the INSTRON tensile test machine and subjected to tensile test. The experimentation was carried out with the INSTRON machine to record the material yield strength values resulting from the welding application as shown in Figure 2. Also, Figure 3 shows the twenty (20) best samples after the tensile test experimental procedure.

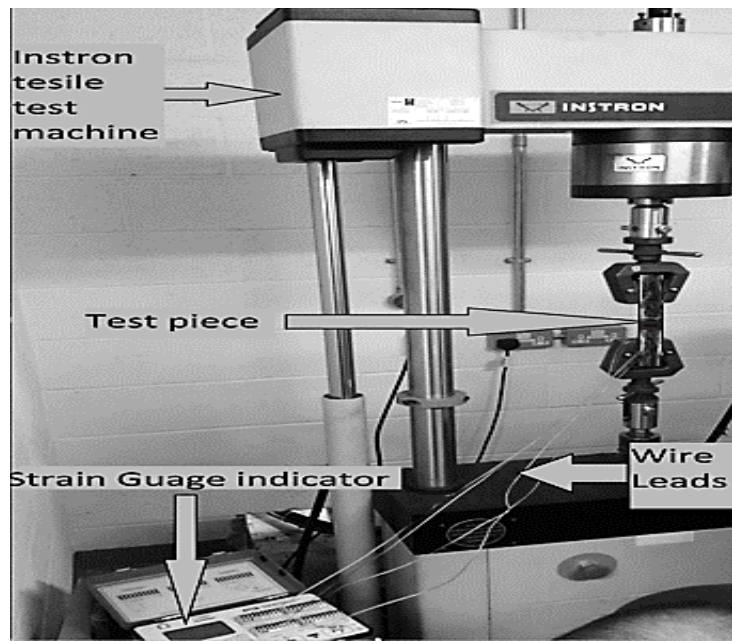


Figure 2. Experimental set-up for specimen mounted on INSTRON tensile test machine



Figure 3. Test samples that have undergone tensile test from INSTRON tensile test machine

2.1. Finite Element Method

A numerical method for resolving boundary value issues related to nonlinear partial differential equations is the finite element method (FEM), commonly referred to as finite element analysis (FEA). The procedure produces approximations of the unknown values at a discrete number of places throughout a specified region. It breaks a complex issue down into little, easier pieces known as finite components in order to solve it. Then, a bigger network of equations that represents the overall issue is constructed using a set of equations that describe the finite elements. Beyond that, the Finite Element Method utilizes variational methods from differential calculus to create a solution by minimizing potential error functions. The Finite Element Method is based on the idea of the Direct Stiffness Method, also known as the Matrix Stiffness Method, which uses the member's stiffness principles for computing thermal stresses, displacements, member forces, and other quantities. To use FEM to welding operations, a simple system must be modelled with a large number of idealized parts connected by nodes. Through the use of the matrix mathematics, the physical equations that determine the reaction of the overall idealized structure are constructed from the simulation of the elemental formations that make up the material's stiffness qualities. When using the finite element approach for structural mechanics, the following procedures were used:

- i. Subdividing the continuum into a finite number of components with properties such as squares, rectangles, triangles, and line segments.
- ii. Choosing important locations on the elements to act as nodes for the application of equilibrium and compatibility requirements.
- iii. Making the assumption that each individual element's displacement functions depend on the nodal values in order to determine the displacements at each generic point.
- iv. Sufficient connection of the stress-strain and strain-displacement relationships inside a certain part.
- v. Calculate an element's stiffness and corresponding nodal loads using the flexibility technique or energy principles.
- vi. Formulating equilibrium equations in terms of the idealized element for each set of dissipated continuum nodes.
- vii. Resolve the nodal displacement equilibrium.
- viii. Calculate the support reactions at constrained nodes in the event of displacement.
- ix. The measurement of strains and stresses at various places within the components.

FEM is typically guided by the principle that says that depending on the input and output parameters, applying boundary conditions (such as force, density, displacement, etc.) beyond the capability of a particular body can lead to numerous circumstances with various configurations. It is well known that the heat produced by the arc on the workpiece surface and the transmission of heat energy into the workpiece are both necessary for successful TIG welding operations. An arc is created when the electrode is pointed toward the workpiece (leaving a tiny air gap), and this arc is utilized to melt and fuse the workpiece at a high temperature. The measurements presented in the finite element CAD model displayed in Figure 4 were used to model the 10 mm mild steel plate used in this investigation using SOLIDWORKS 2021. With SOLIDWORKS Premium, the simulation was run.

The simulation was performed using the Thermal Simulation program. With the findings of the original research serving as a sensor, a design study was conducted. Weld dilution answers were given for a total of fifteen runs that were completed. Eight bodies make up the model. The parent metal is represented by two bodies, and the shape of the weld bead is represented by the other smaller bodies. A 60 X 40 X 10 mm flat plate was the size of the CAD model, as illustrated in Figure 4. Table 3 presents details of the thermal loads used in the analysis. Table 4 tabulates details of the contacts used in the analysis. Table 5 presents details of the sensors used in the analysis. Table 6 presents details of the mesh used in the study.

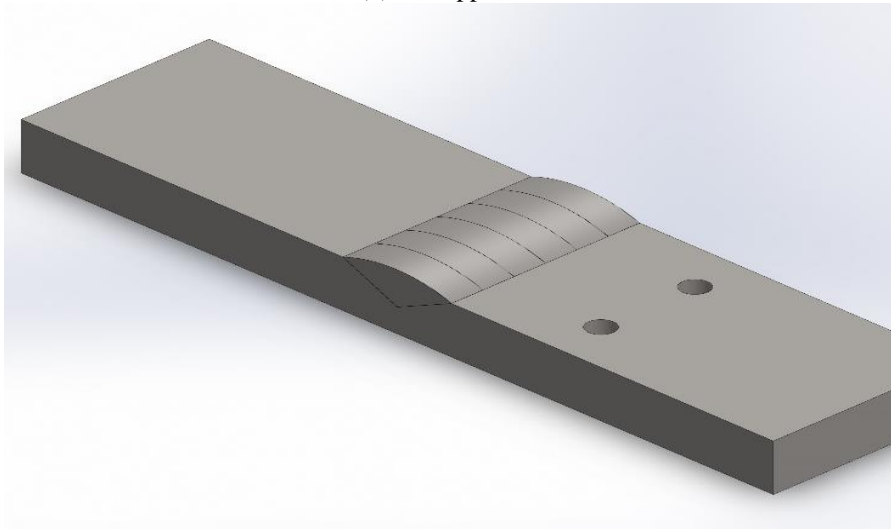
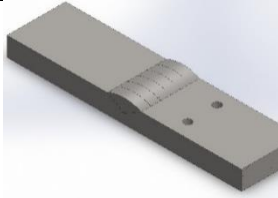
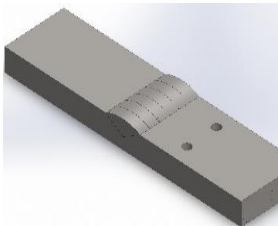
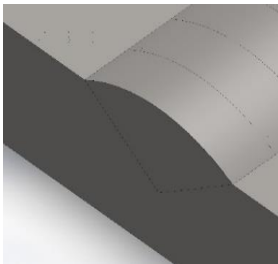
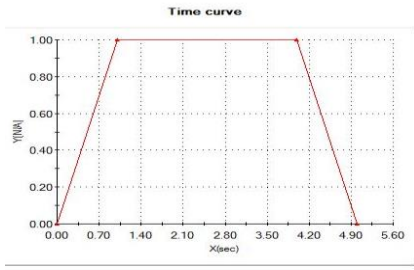
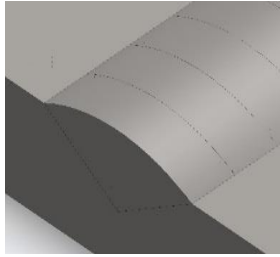


Figure 4. CAD model of low carbon steel plate

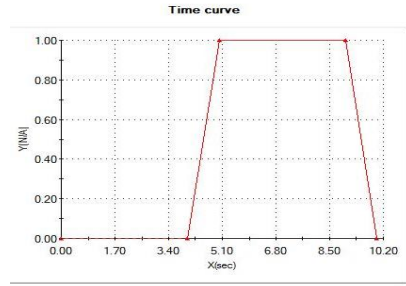
Table 3: Details of thermal loads employed in the analysis

Load name	Load Image	Load Details	Function Curve
Temperature -1		Entities: 15 face(s) Initial temperature: 30°C	
Convection-1		Entities: 15 face(s) Convection Coefficient: 50 W/(m ² .K) Time variation: Off Temperature variation: Off Bulk Ambient Temperature: 28 Kelvin Time variation: Off	
Heat Power- 1		Entities: 5 face(s) Heat Power Value: 1300 W Time variation: on	 <p style="text-align: center;">Time curve</p>

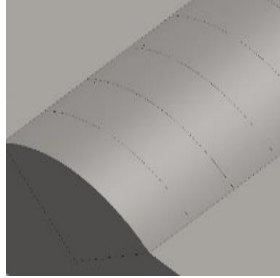
**Heat Power-
2**



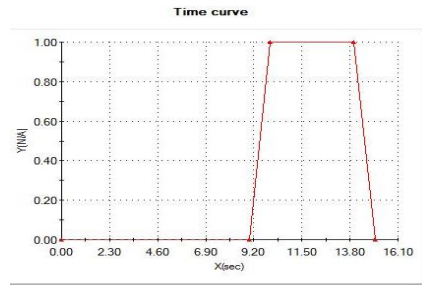
Entities: 5 face(s)
Heat Power Value:
1300 W
Time variation: on



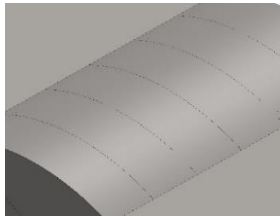
**Heat Power-
3**



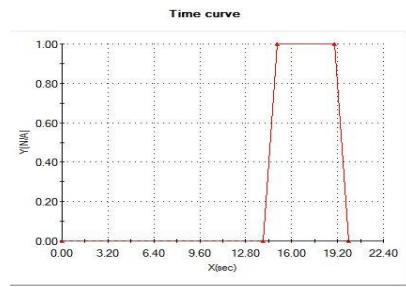
Entities: 5 face(s)
Heat Power Value:
1300 W
Time variation: on



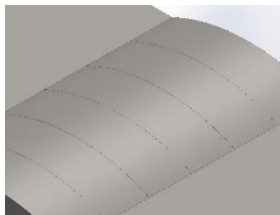
**Heat Power-
4**



Entities: 5 face(s)
Heat Power Value:
1300 W
Time variation: on



**Heat Power-
5**



Entities: 5 face(s)
Heat Power Value:
1300 W
Time variation: on

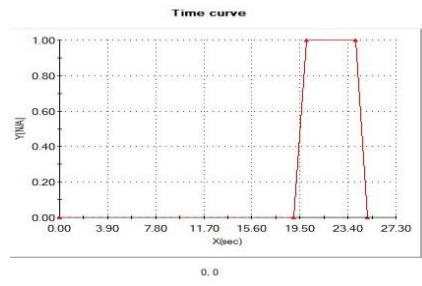
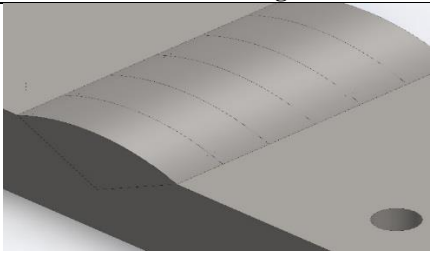
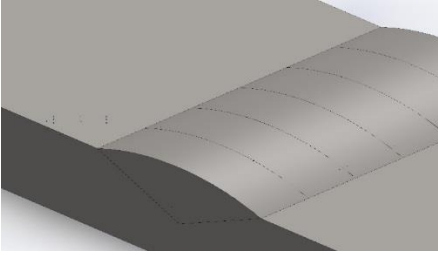
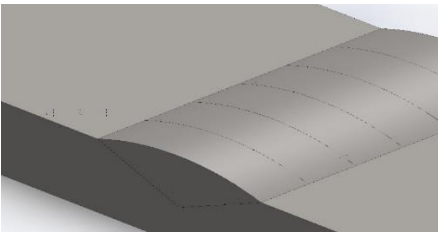
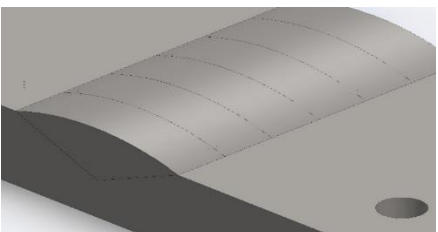
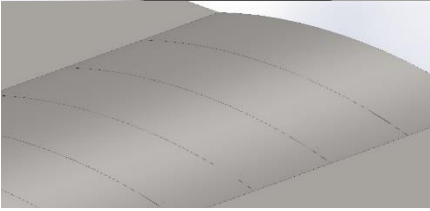
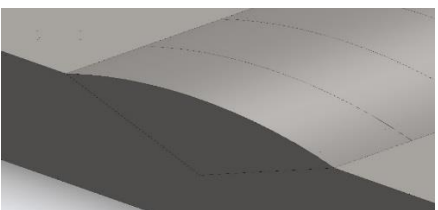
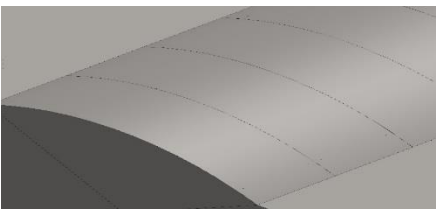


Table 4: Details of contact information employed in the analysis

Contact	Contact Image	Contact Properties
Contact Set-1		Type: Bonded contact pair Entities: 2 face(s)
Contact Set-2		Type: Bonded contact pair Entities: 6 face(s)
Contact Set-3		Type: Bonded contact pair Entities: 2 face(s)
Contact Set-4		Type: Bonded contact pair Entities: 6 face(s)
Contact Set-5		Type: Bonded contact pair Entities: 2 face(s)
Contact Set-6		Type: Bonded contact pair Entities: 2 face(s)
Contact Set-7		Type: Bonded contact pair Entities: 2 face(s)

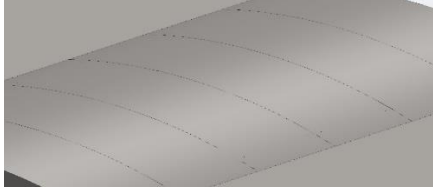
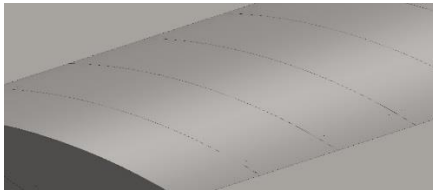
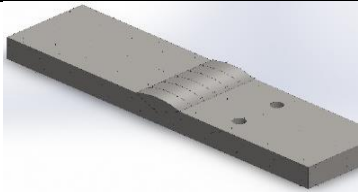
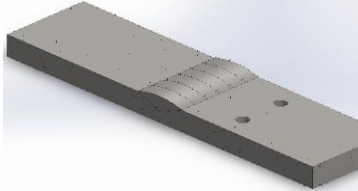
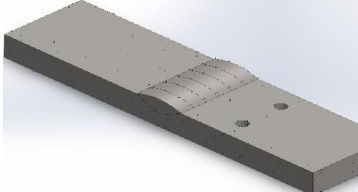
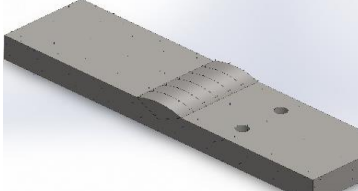
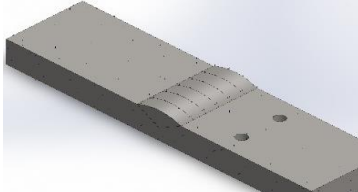
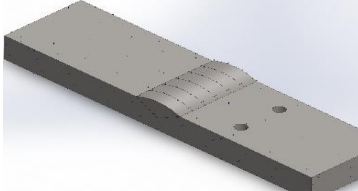
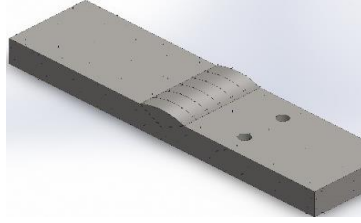
Contact Set-8		Type: Bonded contact pair Entities: 2 face(s)
Contact Set-9		Type: Bonded contact pair Entities: 2 face(s)

Table 5: Sensor details employed in the analysis

Sensor name	Location	Sensor Details
Thermal 1		Value: 937.613 Celsius Result: Thermal Component: Temperature Criterion : Model Average Step Criterion : Across all Steps
Thermal 2		Value: 937.613 Celsius Result: Thermal Component: Temperature Criterion: Model Average Step Criterion: Across all Steps
Thermal 3		Value: Result: Thermal Component: Temperature Criterion: Model Average Step Criterion: Across all Steps
Thermal 4		Value : Result: Thermal Component: Temperature Criterion: Model Average Step Criterion: Across all Steps
Thermal 5		Value: 5165.18 Celsius Result: Thermal Component: Temperature Criterion : Model Average Step Criterion: Across all Steps
Thermal 6		Value: 1321.45 Celsius Result: Thermal Component: Temperature Criterion: Model Average Step Criterion: Across all Steps

Thermal 7

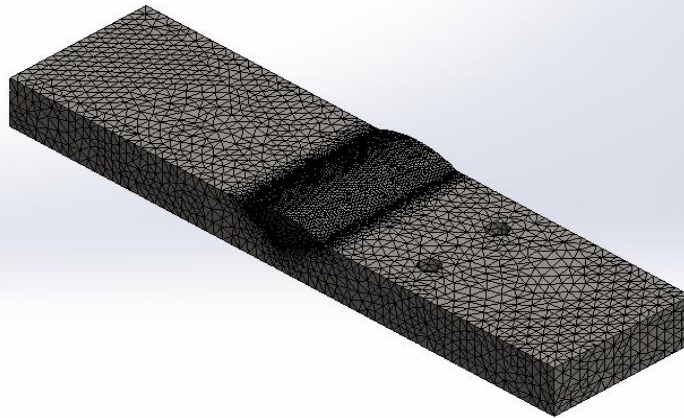



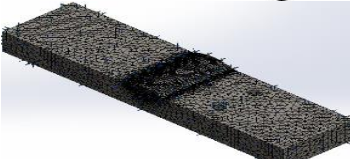
Value: 1321.45 Celsius
Result: Thermal
Component: Temperature
Criterion: Model Average
Step Criterion: Across all Steps

Table 6: Mesh information employed in the analysis

Mesh	Information
Mesh type	Solid Mesh
Mesher Used	Curvature based mesh
Jacobian points	4 Points
Maximum element size	2.11665 mm
Minimum element size	0.705542 mm
Mesh Quality	High
Re-mesh failed parts with incompatible mesh	Off
Total Nodes	275719
Total Elements	198159
Maximum Aspect Ratio	4.4622
% of elements with Aspect Ratio < 3	99.7
% of elements with Aspect Ratio > 10	0
% of distorted elements(Jacobian)	0
Time to complete mesh (hh:mm:ss)	00:00:27

Model name: GTAW
Study name: Thermal 1(-Default-)
Mesh type: Solid mesh



Mesh Control Name	Mesh Control Image	Mesh Control Details
Control-1		Entities: 7 edge(s), 2 face(s) Units: mm Size: 0.332403 Ratio: 1.5
Control-2		Entities: 6 component(s) Units: mm Size: 0.664806 Ratio: 1.5

3. Results and Discussions

Having conducted the welding experiment using TIG welding technique and the finite element modelling and simulation sequence, the results obtained were tabulated. Thus, Table 7 represent the results obtained from experimental welding procedure while Table 8 represents welding results obtained from finite element approach.

Table 7: Results obtained from the experimental welding procedure

Weld Runs	Current (amps)	Voltage (V)	Gas flow rate (litters/min)	Welding speed (mm/min)	Welding Temperature (°C)	Yield Strength (MPa)
1	180	21.00	19.00	3.75	1400	464.47
2	183	18.00	19.00	3.75	1694	452.872
3	185	18.50	19.00	3.75	1500	453.243
4	190	19.00	19.00	3.75	1450	445.975
5	195	21.50	19.00	3.75	1406	470.713
6	200	20.00	19.00	3.75	1500	437.241
7	205	20.50	19.00	3.75	2152	445.216
8	210	21.00	19.00	3.75	1350	446.519
9	213	18.00	19.00	3.75	1350	455.236
10	215	18.50	19.00	3.75	2790	442.875
11	218	19.00	19.00	3.75	1220	434.985
12	221	21.50	19.00	3.75	1360	439.342
13	225	20.00	19.00	3.75	2500	436.719
14	225	20.50	19.00	3.75	1240	444.212
15	240	21.00	19.00	3.75	1610	456.364
16	228	18.00	19.00	3.75	1180	437.562
17	230	18.50	19.00	3.75	1240	453.431
18	230	19.00	19.00	3.75	1483	464.619
19	235	21.50	19.00	3.75	1320	430.247
20	225	20.00	19.00	3.75	1250	449.853

Table 8: Welding results obtained from the finite element approach

Weld Runs	Current (amps)	Voltage (V)	Gas flow rate (litters/min)	Welding speed (mm/min)	Welding Temperature (°C)	Yield Strength (MPa)
1	180	21.00	19.00	3.75	1420	466.420
2	183	18.00	19.00	3.75	1703	457.783
3	185	18.50	19.00	3.75	1450	460.240
4	190	19.00	19.00	3.75	1430	442.345
5	195	21.50	19.00	3.75	1391	478.724
6	200	20.00	19.00	3.75	1450	440.216
7	205	20.50	19.00	3.75	2200	452.836
8	210	21.00	19.00	3.75	1320	452.719
9	213	18.00	19.00	3.75	1325	463.228
10	215	18.50	19.00	3.75	2834	447.707
11	218	19.00	19.00	3.75	1240	438.765
12	221	21.50	19.00	3.75	1350	447.242
13	225	20.00	19.00	3.75	2596	443.520
14	225	20.50	19.00	3.75	1280	450.215
15	240	21.00	19.00	3.75	1667	464.738
16	228	18.00	19.00	3.75	1200	442.560
17	230	18.50	19.00	3.75	1270	461.426
18	230	19.00	19.00	3.75	1516	470.864
19	235	21.50	19.00	3.75	1360	435.341
20	225	20.00	19.00	3.75	1300	458.751

As observed in Figures 5 and 6, a significant correlation is established between the FEM modelled welding temperature and the experimentally measured welding temperature as well as FEM modelled yield strength (tensile) and the experimentally determined yield strength (tensile). This can be observed in the pattern of the plots shown Figure 5 and 6. For example, two highest values of experimentally determined welding temperature and yield strength were 2790 and 2500°C both observed at weld run No. 10 and 13 as well as 470.713 and 464.619MPa, both observed at weld run No. 5 and 18. Also, two highest values of finite element modelled welding temperature and yield strength were 2834 and 2596 °C both observed at weld run No. 10 and 13 as well as 478.724 and 470.864MPa, both observed at weld run No. 5 and 18. This implies that Finite Element Method can be adopted as an effective tool in modelling and prediction of TIG welding related parameters [22, 23] such as welding temperature distribution and yield strength (tensile) variations on welded materials. All the plots exhibited one common trend depicting coherent increase in welding temperature and yield strength (tensile) which further buttress the claim stated earlier that welding temperature and yield strength increase in pari passu as graphically illustrated in Figures 5 and 6. It can be observed from the plots in Figure 5 and 6 that welding temperature and yield strength measured at each point of welding temperature varied closely with one another depending on whether the welding temperature decreases or increases.

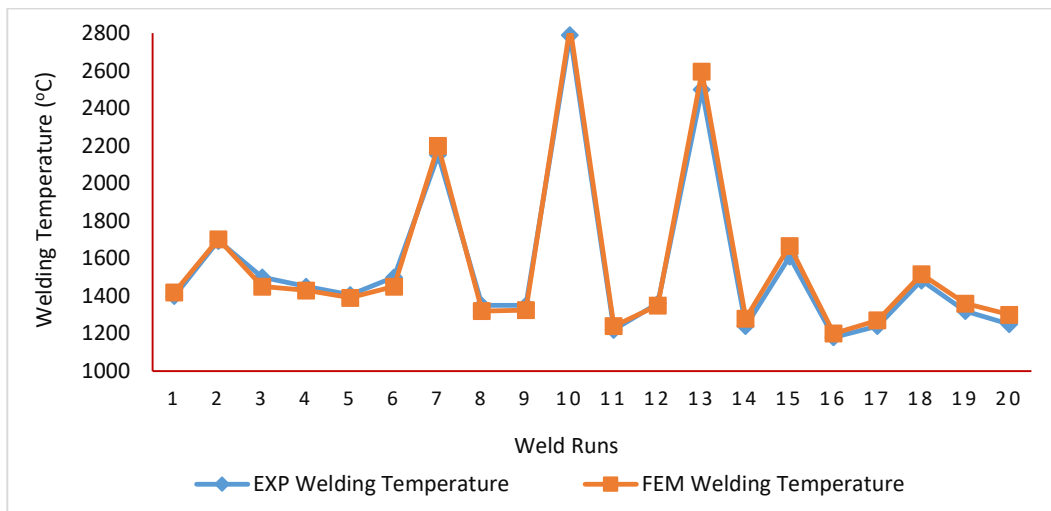


Figure 5. Experimental and FEM results for welding temperature

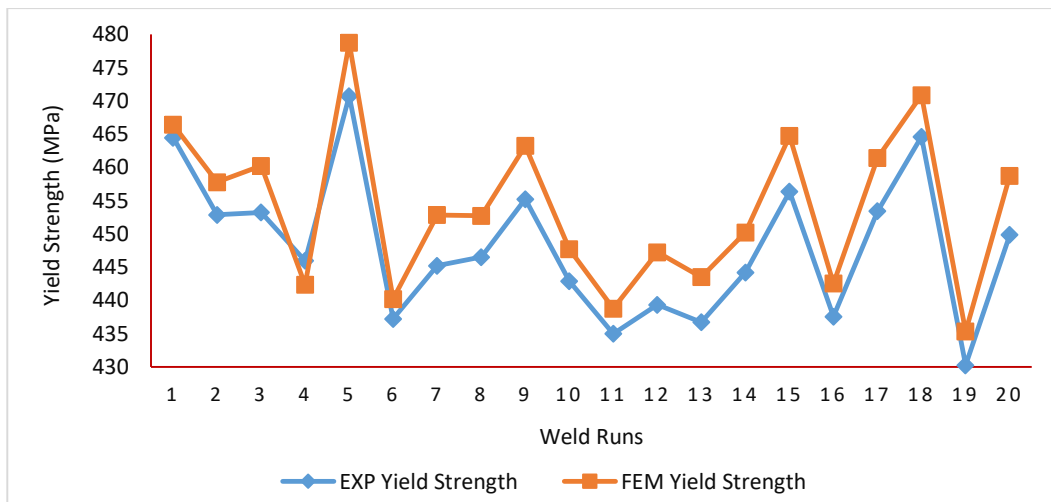


Figure 6. Experimental and FEM results for yield strength

The 3D simulation models of AISI 1018 low carbon steel plate depicted the multiplex phase transformations resulting from the TIG welding input variables and heat transfer due to welding temperature. As a result, at the beginning of the simulation operation that produced the necessary nodal temperature record, Solid Works Finite Element Solver (FES) was deployed with transient cum nonlinear thermal solution. This solution will be precipitated on the convention of heat conduction, radiative boundary conditions, and convection. Similar to this, by using a curvature-typed screen as the lacework and FFEPlus as the solvent in the thermal solution, the separation of the metallic flat plate with screen refinement by the side of the welded zone will make it easier to predict the temperature and its distribution of residual stress, which corresponds to the steel plate across its section. Additionally, it was evident that the dependent analysis was established using the temperature profiles as thermal loads to determine the residual stress zones. The residual stress criteria in the steel plate specimen make the use of FEM for thermal analysis a feasible platform. In reality, the welding process runs on a thermal cycle that starts with heat transfer from the welded area (Heat Affected Zone, or HAZ), followed by heat that spreads throughout the weldment and the entire welded plate.

On the other hand, another finding was that the maximum welding temperature and yield strength regions on each finite element simulation weld profile were found to be located near the fusion zones that were divided by the flat plates' horizontal and vertical planes, where the two specimens were TIG welded together. The present investigation uses two cold metal plates to regulate the deposition of molten metal during the TIG welding process. It may be inferred that each welding procedure (performed sequentially) resulted in the weld metal contracting upon cooling at the welded connection. The increase in the thermal cycle surrounding the weldment, which happened at the heat input, is the resultant consequence.

Figures 7a-b to 13a-b show the thermal cycle on which the welding profile which is characterised by heat transfer and distribution across the weld pool and welding profile for yield strength, of which both profiles were developed from SOLIDWORKS (2021 version) computational tool using finite element method as mentioned earlier. Welding temperature found on the profiles indicates that temperature gradients ranging from 1391-2834°C were employed in the process while yield strength values found on the same profiles ranged from 443.520-478.724MPa. The temperature profiles are presented in Figures 7a, 8a, 9a, 10a, 11a, 12a and 13a while the yield strength profiles are presented in Figures 7b, 8b, 9b, 10b, 11b, 12b and 13b are also placed side by side with the temperature profiles.

Each of the Figures has a legend characterized by different colours, which has its indication related to the material behaviour when exposed to welding heat. From the order in which the colours appear on the weld profile legend, it can be observed that red colours appear at the top while royal blue colours appear at the bottom. Welding temperature and yield strength values on the weld profiles include red colours, royal blue colours and other colours. Welding temperature and yield strength values associated with red colour signifies the maximum output responses while Welding temperature and yield strength values attached to royal blue colour signifies minimum output responses. However, values for the two output responses linked to orange, lemon, green and sky-blue colours have their severity. In other words, if the values are considered from ascending order which is from red colour, it reduces until it gets to the least value represented by blue and vice versa. According to certain research, the amount of thermal stress in AISI 1020 Low Carbon Steel Plate that has been TIG welded to it increases proportionally with welding temperature. In other words, increasing the welding temperature causes the distribution of thermal stress along the fusion zone of the weldment to rise [24, 25]. It was underlined by Mishchenko and Scotti [26] that the thermal stress distribution gradually diminishes throughout the HAZ. By varying the temperature gradients around the weld region with sufficient heat needs at regular intervals, such situations can be minimized [27]. On the other hand, Owunna and Ikpe [28] found that bead width increased when welding temperature rose owing to heat input from the current and that variations in bead width were also influenced by the voltage at varied rates (21V, 25V, and 19V).

According to several researches, weld metal's tensile and yield strengths decrease as heat input levels rise. A greater heat input causes a slower cooling rate, which results in weldments with lower yield strength. In other words, the sluggish cooling that is linked with it causes the HAZ to produce austenite grains, which results in poor toughness [29, 30, 31, 32]. The efficiency of the welding process and arc energy are key factors in the heat input for GTAW. Thermal effects on the weld metal and heat-affected zone (HAZ) are caused by the heat input during welding. Conduction, convection, and ohmic heating are some of the heat transmission methods that are used to heat the weld pool and the droplet.

Grain growth replaced both coarse and fine grain zones in reheated regions due to a decrease in tensile strength and an increase in heat input. Larger cellular dendritic cell spacing, less acicular ferrite, and coarser acicular ferrite laths are the effects of increasing heat input. Because of this, a high heat input causes cooling to occur more slowly, but it also produces highly coarse HAZ, which has poor strength and toughness in the weldment. Additionally, a high heat input causes pro-eutectoid ferrite to replace acicular ferrite, increasing the bead size and breadth of the columnar grains at the expense of the yield strength and toughness qualities. When welding, a high heat input causes the following:

- i. Lessened yield strength;
- ii. Lessened weld metal toughness;
- iii. inadequate HAZ toughness
- iv. Large-grain ferrite
- v. Weld and HAZ hardness reduction

Rapid cooling and a high toughness microstructure are both products of low heat input welding. As a result, welding with little heat input might lead to:

- i. Optimized weld metal and HAZ toughness
- ii. Enhancement of yield strength
- iii. Improvement in acicular ferrite formation
- iv. weld hardness improvement

Welding heat input is the product of current and voltage divided by travel speed. Therefore, to control the welding heat input, values of the welding current and voltage were regulated in the lower range while the travel speed was in the higher range. Also, the welding procedure was conducted by stringer beads, as they helped regulate the travel speed on faster pairs. It was observed that weaving brought about a reduction in the welding travel speed which in turn increased the welding heat input.

However as observed in this study (see Figure 8b, a maximum yield strength (tensile) value of 478.724MPa represented by red colour was produced by a welding temperature of 1391°C in Figure 8a.

A higher yield strength value which was close but less than the maximum yield strength-tensile (478.724MPa as shown in Figure 8b) by 7.86MPa was 470.864Mpa as shown in Figure 13b, produced by welding temperature of 1516°C as shown in Figure 13a.

Moreover, the maximum welding temperature of 2834°C (see Figure 10a) represented by red colour produced a yield strength value of 447.706 MPa as illustrated in Figure 10b. A higher welding temperature value which was close but less than the maximum welding temperature (2834°C as shown in Figure 10a) by 238°C was 2596°C (see Figure 11a), and produced a yield strength value of 443.520MPa as shown in Figure 11b.

While the temperature and yield strength profiles indicate that low welding temperature can produce increased or high yield strength values, it can also be observed in the comprehensive results obtained

from the experimental and FEM approach presented earlier in Tables 7 and 8 that; the condition is a function of other welding input variables coming into play. In other words, it was observed that varying the welding current, arc voltage, gas flow rate and welding speed during welding experiments and finite element simulation can result in alternating output responses. This implies that the output responses depend on the variations of input variables which can directly or indirectly influence the welding outcome. For example, it is also observed in the FEM results in Table 8 that welding temperatures of 1667, 1420, 1703 and 1450°C produced yield strength values of 464.738, 466.420, 457.783 and 460.240MPa respectively. Figures 7a-b to 13a-b are selected finite element simulation models representing welding profiles for temperature distribution on the welded workpiece and tensile yielding effect on the material. It can be observed that each profile has a region characterised by minimum and maximum welding temperature and yield strength. A close observation of these regions in each profile indicated that maximum temperature occurred around the weld pool while the maximum yield strength value also occurred around the welded region or fusion zone. Comparatively, the FEM simulated yield strength and experimentally determined yield strength fell in the range 478.724-435.341 and 430.247-470.713MPa, which are quite higher than the yield strength obtained from the original AISI 1018 samples prior to welding. This is a clear indication that the fusion zone is stronger than the parent metal.

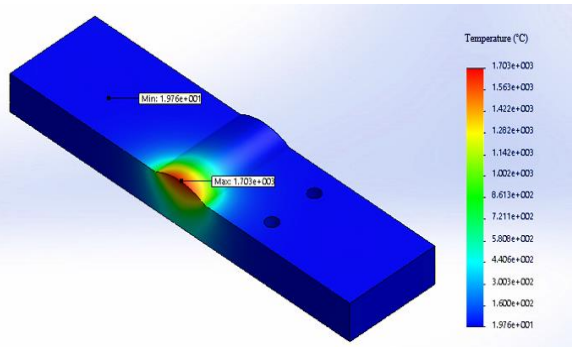


Figure 7a. Weld profile at max temperature of 1703 °C

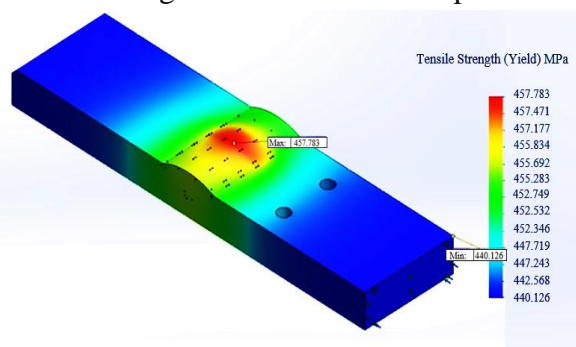


Figure 7b. Weld profile at max temperature 457.783 MPa

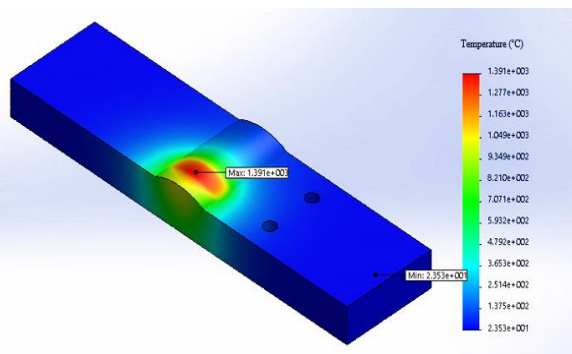


Figure 8a. Weld profile at max temperature of 1391 °C

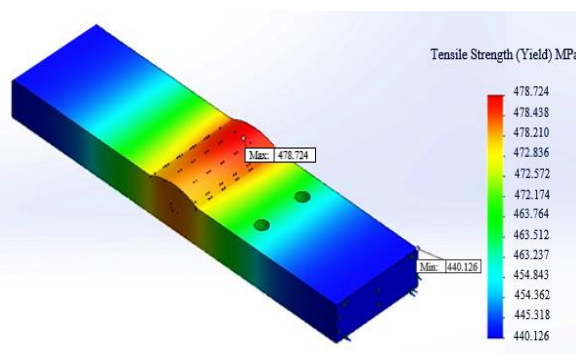


Figure 8b. Weld profile at max temperature 478.724 MPa

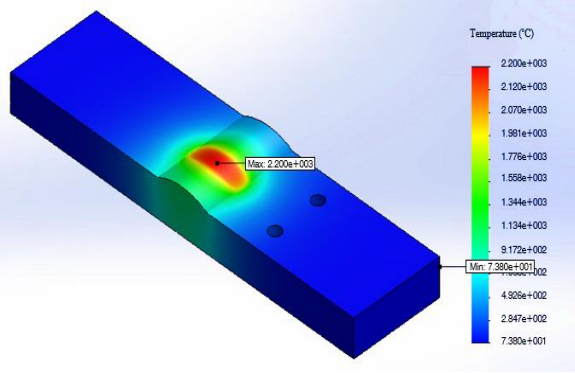


Figure 9a. Weld profile at max temperature of 2200 °C

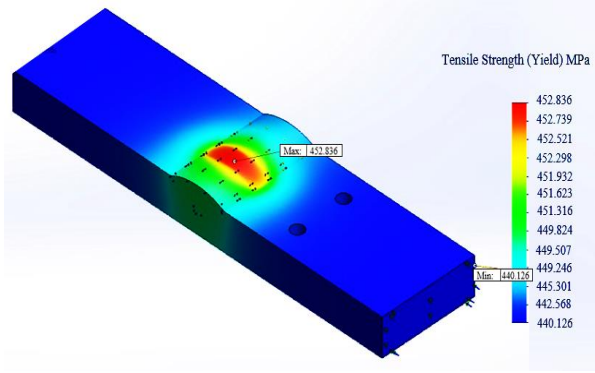


Figure 9b. Weld profile at max temperature 452.836 MPa

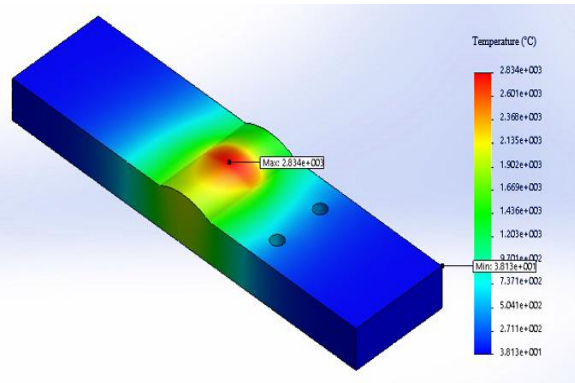


Figure 10a. Weld profile at max temperature of 2834 °C

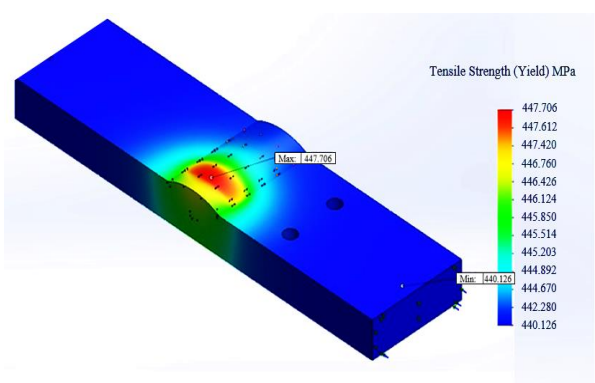


Figure 10b. Weld profile at max 447.706MPa

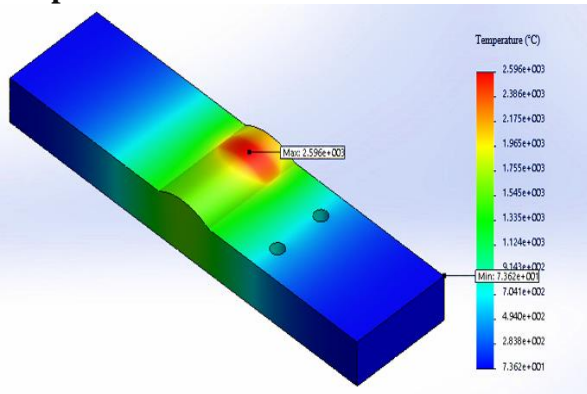


Figure 11a. Weld profile at max temperature of 2596 °C

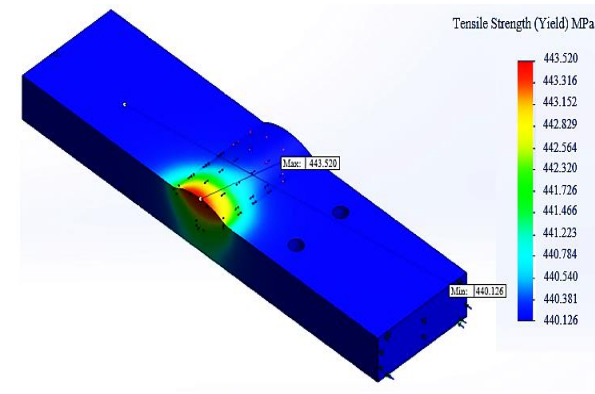


Figure 11b. Weld profile at max 443.520MPa

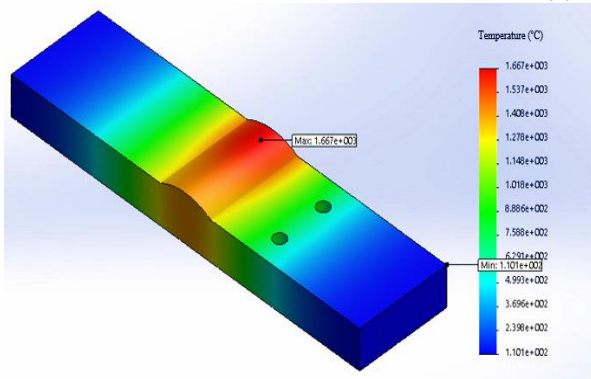


Figure 12a. Weld profile at max temperature of 1667°C

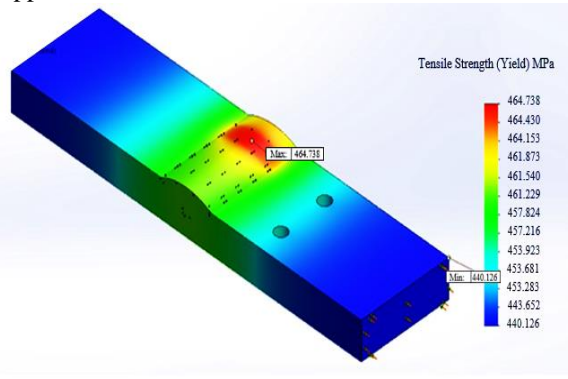


Figure 12b. Weld profile at max 464.738MPa

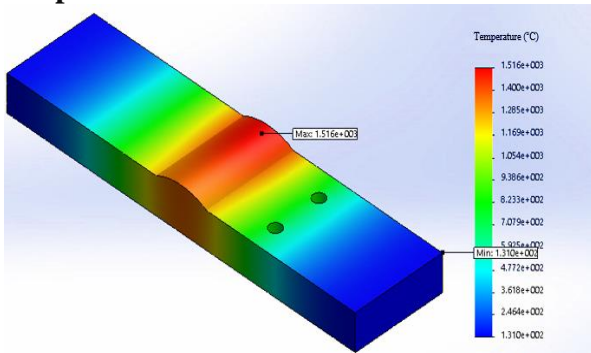


Figure 13a. Weld profile at max temperature of 1516°C

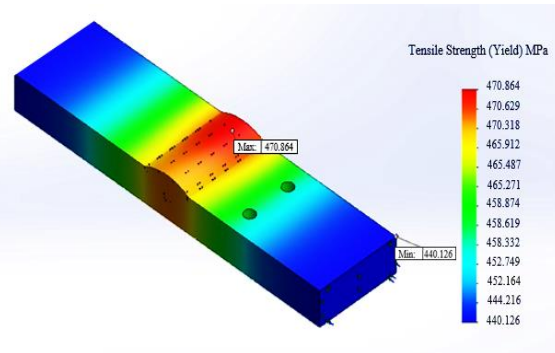


Figure 13b. Weld profile at max 470.864MPa

4. Conclusion

In this study, thermal transient simulation was carried out using SolidWorks computational tool to determine the thermo-mechanical transient behavior of mild steel plate practically agglutinated by gas tungsten arc welding technique. It was observed that varying the welding current, arc voltage, gas flow rate and welding speed during welding experiment and finite element simulation can result in alternating output responses due heat transfer through conduction. There are no hard and fast rules for choosing between high heat and low heat, or between utilizing argon or CO₂ as a shielding gas. Everything is dependent on the demands and specifications of the particular application. That makes it important for welding operators to have broad understanding of the relationship between these input variables, and the effect each has on the thermo-mechanical properties of the weld. Therefore, the knowledge on how to regulate the input variables is very essential to achieving the desired output response, while it also assist welding operators in making specific choices that can result in optimum welding outputs. Hence, selection of adequate welding parameters such as welding current of 195A, voltage of 21.50V, gas flow rate of 19 L/min and welding speed of 3.75 experimentally produced welding temperature of 1406°C and yield strength (tensile) of 470.713 MPa while the same welding current of 195 A, voltage of 21.50 V, gas flow rate of 19 L/min and welding speed of 3.75 computationally produced welding temperature of 1391°C and yield strength (tensile) of 478.724 MPa, indicating that FEM is an effective tool that can be employed in simulation of thermo-mechanically related models

Nomenclature

AISI	American iron and steel institute
CAD	Computer Aided Design
CCD	Central Composite Design
DOE	Design of Experiment
GTAW	Gas Tungsten Arc Welding
HAZ	Heat Affected Zone
FE	Finite Element
DIC	Digital Image Correlation
FEA	Finite Element Analysis
FEM	Finite Element Method
FES	Finite Element Solver
RSM	Response Surface Methodology
SCZ	Stress Critical Zone
TIG	Tungsten Inert Gas
UTS	Ultimate tensile Strength
3D	Three dimension

References

- [1] K. Kalita, D. Burande, R. K. Ghadai, and S. Chakraborty (2023). Finite Element Modelling, Predictive Modelling and Optimization of Metal Inert Gas, Tungsten Inert Gas and Friction Stir Welding Processes: A Comprehensive Review. *Arch. Comput. Meth. Eng.*, Vol.30(1), pp.271-299.
- [2] A. Ikpe, I. Owunna and I. Ememobong (2017). Effects of Arc Voltage and Welding Current on the Arc Length of Tungsten Inert Gas Welding (TIG). *Int. J. of Eng. Tech.* Vol.3(4), pp.213-221.
- [3] M. Zubairuddin, S. K. Albert, M. Vasudevan, S. Mahadevan, V. Chaudhari and V. K. Suri (2017). Numerical simulation of multi-pass GTA welding of grade 91 steel. *J. Mfg. Proc.*, Vol.27, pp.87-97.
- [4] A. Shiri, and A. Heidari (2019). Investigating the effect of joint geometry of the gas tungsten arc welding process on the residual stress and distortion using the finite element method. *J. Sld. Mech.*, Vol.11(4), pp.736-746.
- [5] K. Agrebi, A. Belhadj and M. Bouhafs (2019). Three-dimensional numerical simulation of a gas tungsten arc welding process. *Int. J. Tech.*, Vol.10(4), pp.689-699.
- [6] C. Wu, C. Wang and J. W. Kim (2021). Welding distortion prediction for multi-seam welded pipe structures using equivalent thermal strain method. *J. of Wldg. Jng.*, Vol.39(4), pp.435-444.
- [7] P. H. Chang and T. L. Teng (2004). Numerical and experimental investigations on the residual stresses of the butt-welded joints. *Comput. Matl. Sci.*, Vol.29(4), pp.511-522.
- [8] A. E. Ikpe and M. Bassey (2023). Modelling and simulation of transient thermal stress distribution across AISI 1018 flat plate at variable welding temperature regime. *J. Eng. Struct. Comput.*, Vol.2(3).
- [9] K. S. Mohan and N. S. Shanmugam (2019). Finite element simulation for tensile and impact test of activated TIG welding of AISI 321 austenitic stainless steel. *Proc. Inst. Mech. Eng., Part L: J. Matl: Des. App.*, Vol.233(11), pp.2323-2334.
- [10] J. J. del Coz Díaz, M. Rodríguez, G. Nieto and D. Castro-Fresno (2010). Comparative analysis of TIG welding distortions between Austenitic and Duplex Stainless Steels by FEM. *App. Therm. Eng.*, Vol.30(16), pp.1-14.
- [11] A. M. Bash (2019). Numerical Simulation of Welding Influence on Tensile Strength and Residual Stress of AISI 304 Butt Joints. *J. Adv. Res. Fld. Mechs. Therm. Sci.*, Vol.64(1), pp.77-91.
- [12] W. Jiang, X. P. Xu, J. M. Gong, and S. T. Tu. (2012). Influence of repair length on residual stress in the repair weld of a clad plate. *Nuc. Eng. Des.*, Vol.246, pp.211-219.
- [13] C. Chen, C. Sing-Ping, Z. Ming-Shan, L. Chi-King and F. Tat-Ching (2019). Welding effect on tensile strength of grade S690Q steel butt joint. *J. Constr. Stl. Res.*, Vol.153, pp.153-168.
- [14] H. Huang, X. Yin, Z. Feng and N. Ma (2019). Finite Element Analysis and In-Situ Measurement of Out-of-Plane Distortion in Thin Plate TIG Welding. *Mat.*, Vol.12(141), pp.1-17.
- [15] I. U. Musa, M. O. Afolayan, O. Afolayan and I. M. Dagwa (2016). Finite Element Model for Predicting Residual Stresses in Shielded Manual Metal Arc Welding of Mild Steel Plates. *Nig. J. Tech.*, Vol.35(1), pp.85-90
- [16] V. García-García, I. Mejía, F. Reyes-Calderón, J. A. Benito and J. M. Cabrera (2020). FE thermo-mechanical simulation of welding residual stresses and distortion in Ti-containing TWIP steel through GTAW process. *J. Mfg. Proc.*, Vol.59, pp.801-815.
- [17] A. E. Ikpe and I. Owunna (2018). Optimization of TIG Welding Input Variables for AISI 1020 Low Carbon Steel Plate Using Response Surface Methodology. *Int. J. Eng. Sci. App.*, Vol.2(3), pp.113-122.

- [18] S. Bhattacharya (2021). Central Composite Design for Response Surface Methodology and Its Application in Pharmacy. Response Surface Methodology in Engineering Science, Kayaroganam, Intechopen Limited, London, United Kingdom.
- [19] I. B. Owunna and A. E. Ikpe (2021). Experimental and Numerical Optimization of Tungsten Inert Gas (TIG) Welding Process Parameters Relative to Mechanical Properties of AISI 1018 Mild Steel Plate. Adv. Eng. Des. Tech, Vol.3, pp.132-145.
- [20] L. Prabhu, S. S. Kumar, S. Krishnamoorthi and S. Prakash, S. (2019). Optimization of Vibration Parameters for Boring Bar Operation by RSM and ANN. Int. J. of Eng. and Adv, Tech, Vol.8(6), pp.2167-2176.
- [21] A. Kumar and R. Gandhinathan (2020). Process Parameters for Metal Inert Gas Welding of Mild Steel by Using Taguchi Technique-A-Review. Int. J. of Mat. Sci and Tech, Vol.10(1), pp.1-14.
- [22] I. Owunna, A. E. Ikpe and J. I. Achebo (2018). 3D Finite Element Modelling of Weld Bead Penetration in Tungsten Inert Gas (TIG) Welding of AISI 1020 Low Carbon Steel Plate. Eur. Mech. Sci, Vol.2(3), pp.96-105.
- [23] I. Owunna, A. E. Ikpe and J. I. Achebo (2018). Temperature and Time Dependent Analysis of Tungsten Inert Gas Welding of Low Carbon Steel Plate using Goldak Model Heat Source. J. App. Sci. Env. Mgmt, Vol22(11), pp.1719-1725.
- [24] I. B. Owunna and A. E. Ikpe (2019) Evaluation of induced residual stresses on AISI 1020 low carbon steel plate from experimental and FEM approach during TIG welding process. J. Mech. Eng. Sci, Vol.13(1), pp.4415-4433.
- [25] I. Owunna and A. E. Ikpe (2019). Finite Element Analysis of Tungsten Inert Gas Welding Temperatures on the Stress Profiles of AISI 1020 Low Carbon Steel Plate. Int. J. of Eng. Tech, Vol.5(2), pp.50-58.
- [26] A. Mishchenko and A. Scotti (2021). Welding thermal stress diagrams as a means of assessing material proneness to residual stresses. J. Mat. Sci. Vol.56, pp.1694-1712.
- [27] B. Yelamsetti and G. Rajyalakshmi (2018). Thermal Stress Analysis of Similar and Dissimilar Welded Joints. UPB Sci. Btt. Ser. Vol.80(4), pp.223-240.
- [28] I. Owunna and A. E. Ikpe (2018). Effects of Parametric Variations on Bead Width of Gas Tungsten Arc Welding of AISI 1020 Low Carbon Steel Plate. Int. J. Eng. Tech. Sci, Vol.5(3), pp.1-13.
- [29] S. c. Moi, P. K. Pal, A. Bandyopadhyay, R. Rudrapati (2019). Effect of Heat Input on the Mechanical and Metallurgical Characteristics of TIG Welded Joints. J. Mech. Eng, Vol.16(2), pp.29-40.
- [30] H. Rojas, A. Molina, S. Valdez, B. Campillo, H. Martínez, A. Sedano and S. Serna (2020). The impact of heat input on the microstructures, fatigue behaviors, and stress lives of TIG-welded 6061-T6 alloy joints. Matl Res. Exp, Vol.7, pp.1-10.
- [31] M. Mician, M. Frátrik and D. Kajánek (2021) Influence of Welding Parameters and Filler Material on the Mechanical Properties of HSLA Steel S960MC Welded Joints. Mtl, Vol.11(305), pp.1-18.
- [32] O. L. Osoba, W. A. Ayoola, Q. A. Adegboju and O. A. Ajibade (2021). Influence of Heat Inputs on Weld Profiles and Mechanical Properties of Carbon and Stainless Steel. Nig. J. Tech. Dev, Vol.18(2), pp.135-143.